

## Stacked-Ring Aromaticity: An Orbital Model

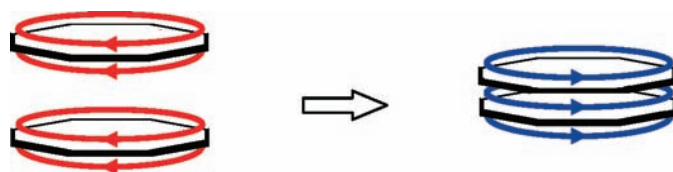
D. E. Bean and P. W. Fowler\*

Department of Chemistry, The University of Sheffield, S3 7HF, United Kingdom

p.w.fowler@sheffield.ac.uk

Received October 20, 2008

## ABSTRACT



Visualization of induced current density using the ipsocentric CHF/CTOCD-DZ/6-31G\*\* approach gives a direct demonstration of the literature proposal of reversal of  $[4n]$ annulene antiaromaticity on stacking cyclooctatetraene (COT) rings into a superphane. Through-space interactions lead to a closed-shell in which paratropicity of planar COT units is quenched, and layered diatropic currents arise from magnetic response of two pairs of frontier orbitals. A general orbital model rationalizes the differences in current between stacked aromatic and antiaromatic rings.

Corminboeuf, Schleyer, and Warner<sup>1</sup> have proposed that stacking of  $4n\pi$ -electron hydrocarbon rings into “superphane”<sup>2</sup> structures can reverse their antiaromaticity. The evidence comes from calculations on methano-bridged structures that display equalized bond lengths and negative NICS values for pairings of both  $4n\pi$  and  $(4n + 2)\pi$  ring systems.<sup>1</sup> The intriguing conclusion is that stacking “along with triplet and Möbius strategies, is the third way to render  $4n\pi$  electron systems aromatic.” On the magnetic criterion, the attribution of aromaticity implies the existence of a diatropic ring current.<sup>3,4</sup> It is now possible to investigate these currents computationally in a direct way.<sup>5–7</sup> In the present work, mapping of contributions to induced current density is used to give an orbital based interpretation of the origin and nature of the aromaticity of these superphane systems, also applicable to multiply stacked arrays of both  $4n\pi$  and  $(4n + 2)\pi$  types.

In the ipsocentric<sup>7</sup> approach, ring currents arise from virtual excitations between occupied and unoccupied molecular orbitals. A translationally (rotationally) active excitation gives rise to a diatropic (paratropic) current.<sup>8</sup> The ipsocentric formulation is used here to map ring current in two hypothetical analogues of known superphane systems<sup>1</sup> ( $[1_6](1,2,3,4,5,6)$ cyclophane and  $[1_8](1,2,3,4,5,6,7,8)$ cyclophane), chosen to exemplify the effects of proximity on magnetic properties, and hence aromaticity, of both  $(4n + 2)\pi$  and  $4n\pi$  systems. The ipsocentric approach is unique in partitioning induced current density into nonredundant orbital contributions, enabling a clear link between molecular electronic structure and ring currents.

Geometries obtained by optimization at the B3LYP/6-311+G\*\* level<sup>1</sup> were used. Benzene- (COT-)based superphanes show maximum  $D_{6h}$  ( $D_{8h}$ ) symmetry, with planar equilateral carbocycles linked by symmetrical  $\text{CH}_2$  bridges with hydrogen atoms in the equatorial plane. Ring bond lengths (1.421 Å (6-cycle), 1.456 Å (8-cycle)) indicate that delocalization survives the partial pyramidalization implied by  $\pi$  orbital axis vectors<sup>9</sup> ( $35.7^\circ$  and  $37.8^\circ$  to the vertical). Ring-to-ring separations (2.305, 2.162 Å) are compatible with

(1) Corminboeuf, C.; Schleyer, P. v. R.; Warner, P. *Org. Lett.* **2007**, *9*, 3263.

(2) Gleiter, R.; Kratz, D. *Acc. Chem. Res.* **1993**, *26*, 311.

(3) Pople, J. A. *J. Chem. Phys.* **1956**, *8*, 397.

(4) Schleyer, P. v. R.; Maerker, C.; Dransfeld, A.; Jiao, H.; Hommes, N. J. R. v. E. *J. Am. Chem. Soc.* **1996**, *118*, 6317.

(5) Keith, T. A.; Bader, R. F. W. *Chem. Phys. Lett.* **1993**, *210*, 223.

(6) Coriani, S.; Lazzeretti, P.; Malagoli, M.; Zanasi, R. *Theor. Chim. Acta.* **1994**, *89*, 181.

(7) Steiner, E.; Fowler, P. W. *J. Phys. Chem. A* **2001**, *105*, 9553.

(8) Steiner, E.; Fowler, P. W. *Chem. Commun.* **2001**, 2220.

(9) Haddon, R. C. *J. Am. Chem. Soc.* **1986**, *108*, 2837.

expected face-to-face repulsion<sup>10</sup> (attraction<sup>1</sup>) between  $[4n + 2]$  ( $[4n]$ ) $\pi$  systems.

The current density induced by a uniform magnetic field along the principal symmetry axis is calculated using the ipsocentric CTODD-DZ<sup>6</sup> formulation, at the CHF/6-31G\*\* level, implemented in the SYSMO program.<sup>11</sup> Current density maps were plotted in three planes perpendicular to the applied field: (i)  $1a_0$  above the top ring, (ii)  $1a_0$  below, and (iii) in the equatorial plane, as indicated in Figure 1. In

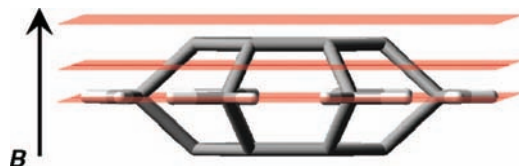


**Figure 1.** Three plotting planes, (i), (ii), and (iii), used in this report.  $B$  is the direction of the external magnetic field.

the maps, contours show the modulus of induced current density and arrows its projection in the plotting plane. Black (dotted) circles represent carbon (hydrogen) positions projected into the plotting plane. Diatropic (paratropic) current, indicating aromaticity (antiaromaticity), is represented by anticlockwise (clockwise) circulation. The ipsocentric method allows decomposition of the total current density into nonredundant contributions from individual molecular orbitals,<sup>7</sup> and a breakdown into explicit contributions from virtual excitations.<sup>12</sup> The maps are compared with standard<sup>8</sup> current-density plots for benzene and COT, and for benzene and COT dimers held in the superphane face-to-face geometries. All calculations of superphane current density were repeated at the B3LYP/6-31G\*\* level<sup>13</sup> but as the maps were essentially unchanged in appearance, only CHF results are reproduced here (see Figure S1, Supporting Information, for a comparison).

Although  $\sigma$ - $\pi$  separation is not enforced in the superphanes, valence molecular orbitals can be assigned approximate  $\pi/\pi^*$ ,  $\sigma/\sigma^*$  character from their energies and symmetries in the  $D_{6h}$  ( $D_{8h}$ ) point group. These assignments agree with simple inspection of orbital density plots. In both systems, HOMO and HOMO - 1 are  $\pi$  orbitals and LUMO and LUMO + 1 are  $\pi^*$ . (In the DFT calculation for  $[1_6]$ (1,2,3,4,5,6)cyclophane, the second  $\pi^*$  orbital is LUMO + 2).

To establish the context, maps of total  $\pi$  current density for benzene and (planar constrained) COT are shown in Figure 2. The response ring currents arising from HOMO-LUMO excitations have been extensively discussed elsewhere.<sup>7,8</sup>

(10) Greenberg, A.; Liebman, J. F. *Strained Organic Molecules*; Academic Press: New York, 1978; Chapter 3.H.4.

(11) Lazzaretti, P.; Zanasi, R. SYSMO Package (University of Modena), 1980. Additional routines: Steiner, E.; Fowler, P. W.; Havenith, R. W. A.; Soncini, A.

(12) Steiner, E.; Soncini, A.; Fowler, P. W. *J. Phys. Chem. A* **2006**, *110*, 12882.

(13) Havenith, R. W. A.; Fowler, P. W. *Chem. Phys. Lett.* **2007**, *449*, 347.

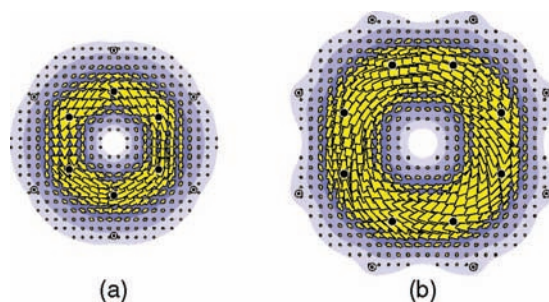


**Figure 2.** Maps showing total  $\pi$  ring current in (a)  $D_{6h}$  benzene and (b)  $D_{4h}$  cyclooctatetraene, plotted at a height of  $1a_0$ .

Benzene shows a purely diatropic  $\pi$  current. Planar COT rings exhibiting paratropic currents are found in “clamped” systems;<sup>14,15</sup> free COT adopts a  $D_{2d}$ -symmetric tub-shaped equilibrium geometry with only localized circulations.<sup>16</sup>

Figure 3 shows current-density maps for  $D_{8h}$   $[1_8]$ (1,2,3,4,5,6,7,8)cyclophane, plotted at three different heights. The top row shows the combined contributions of  $\pi$  HOMO and  $\pi$  HOMO - 1 pairs (the only orbitals to contribute significantly to the  $\pi$  current). These contribute a distinct diatropic ring current at all heights, confirming that the stacking of the two antiaromatic rings does indeed give rise to aromaticity on the ring-current criterion.

In detail, distribution of  $\pi$  current varies with height. Above the top ring, the maximum current occurs outside the circle of carbon positions but, as the plotting plane descends through the molecule, it moves inside the circle and becomes stronger. Its magnitude is indicated by  $j_{\max}$  (the maximum current modulus taken over the plotting plane) and in the three planes,  $j_{\max}$  for the combined  $\pi$   $e_{2g}$  HOMO and  $\pi$   $e_{1g}$  HOMO - 1 orbital contributions is, respectively, 96%, 146%, and 48% of the standard  $\pi$  current in benzene (calculated in the same approach for a height of  $1a_0$ ). In the nodal equatorial plane, the  $e_{1g}$  contribution vanishes. The “hourglass” distribution is consistent with pyramidalisation of the  $p_{\pi}$  atomic orbitals. Survival of significant current in the equatorial plane is an indication of through-space delocalization of the  $\pi$  electrons, consistent with the attribution of “3D aromaticity” to this system by Corminboeuf et al.<sup>1</sup>

Significant orbital contributions from occupied orbitals arise from the  $e_{2g}$  HOMO and  $e_{1g}$  HOMO - 1 pairs. Each of these is attributable semiquantitatively to a single virtual  $\pi$ - $\pi^*$  excitation, to  $e_{3u}$  LUMO + 1 from  $e_{2g}$  HOMO and  $e_{2u}$  LUMO from  $e_{1g}$  HOMO - 1 (see Figure S3, Supporting Information, where 94%, 92% and 82% of the maximum  $\pi$  current at the three plotting heights is recovered by including the lowest  $e_{2u}$  and  $e_{3u}$  virtual orbitals). This is the clue to the pictorial model constructed below.

(14) Matsuura, A.; Komatsu, K. *J. Am. Chem. Soc.* **2001**, *123*, 1768.

(15) Fowler, P. W.; Havenith, R. W. A.; Jenneskens, L. W.; Soncini, A.; Steiner, E. *Angew. Chem., Int. Ed.* **2002**, *41*, 1558.

(16) Havenith, R. W. A.; Fowler, P. W.; Jenneskens, L. W. *Org. Lett.* **2006**, *8*, 1255.

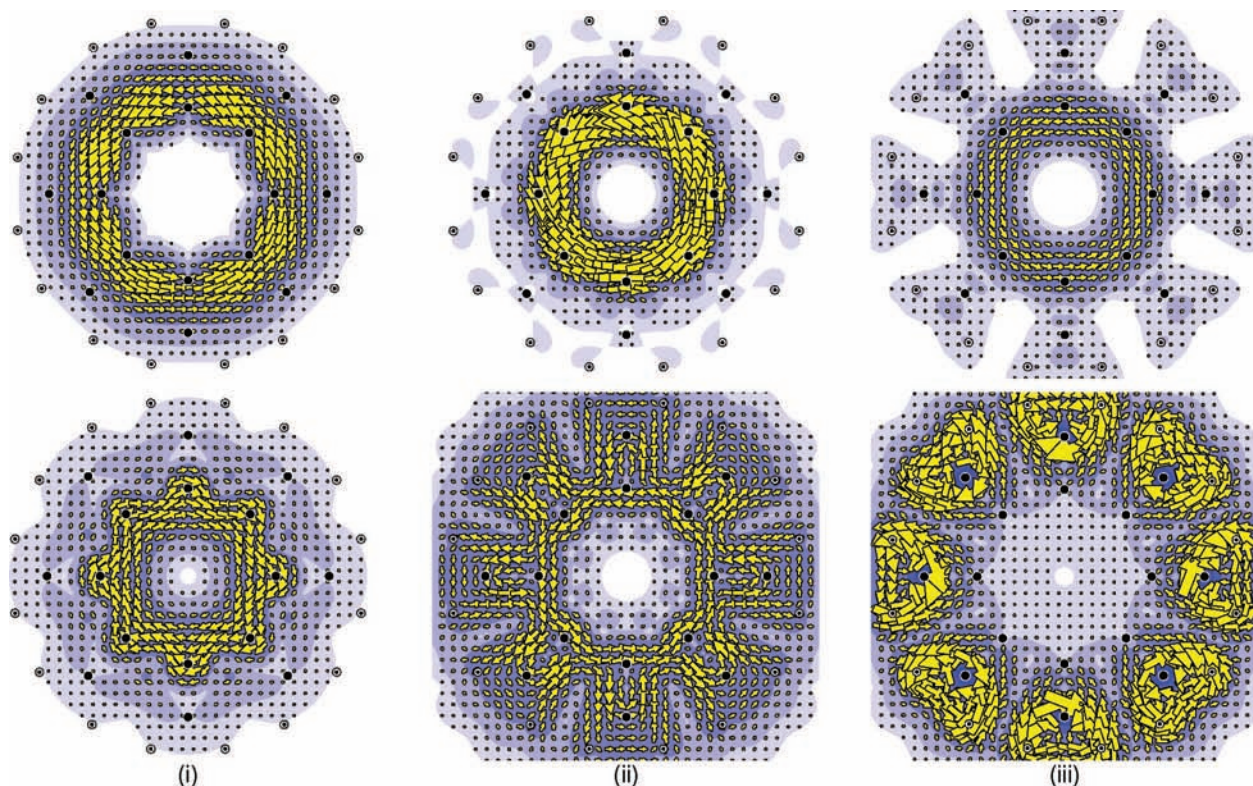


**Figure 3.** Current–density maps for the  $D_{8h}$  superphane. The first row shows the contribution to current density from electrons in the doubly degenerate  $e_{2g}$  HOMO and  $e_{1g}$  HOMO – 1, and the second row shows the contribution from electrons in all valence  $\sigma$ -orbitals. Columns (i)–(iii) refer to the three plotting planes. In the valence  $\sigma$  map at height (iii), large arrows of the bridging carbon cores are omitted for clarity.

The main features of these  $\pi$  current maps arise from through-space interaction, not  $\text{CH}_2$ -bridge mediation, as can be seen from comparison with maps for a constrained COT dimer with the same ring geometry as in the superphane. The plots 1a<sub>0</sub> above and below the ring are more similar, as pyramidalization has disappeared, but the triple-decker diatropic current remains, with strength similar to that in the superphane itself (see Figure S2(b), Supporting Information).

The  $\sigma$ -valence maps in Figure 3 show strong variation between the three plotting planes, ranging from a paratropic circulation associated with the ring interior, through a complex pattern of diatropic circulations, to a sum of localized circulations associated with  $\text{CH}_2$  groups. These patterns are readily understood in terms of superposition of localized  $\sigma$  bond circulations, allowing for the tilt imparted to the  $\sigma$  bonds of the ring by pyramidalization, and the angles at which the plotting planes cut C–C bonds. All features have equivalents in  $\sigma$  frameworks of conventional aromatic systems.<sup>7</sup>

A similar picture applies when two aromatic rings are stacked. Figure S4 (Supporting Information) shows current–density maps of the benzene-based superphane. The results are analogous with those of the COT-based system. A diatropic current is seen, with the same “hourglass” distribution. The  $j_{\text{max}}$  values are, respectively, 73%, 146%, and 23% of the standard benzene current indicating the current in the

central plane is weaker than in the COT analogue. Again, only two pairs of molecular orbitals,  $e_{1g}$  HOMO and  $e_{1u}$  HOMO-1, contribute significantly to the  $\pi$  current, each contribution dominated by a single transition:  $e_{1u}$  to  $e_{2g}$  LUMO and  $e_{1g}$  to  $e_{2u}$  LUMO + 1; similar contributions are found in the constrained dimer (Figure S2, Supporting Information). The significant difference between COT- and benzene-superphanes is that diatropicity in the former entails reversal, in the latter retention, of monomer character.

As mentioned above, the ipsocentric approach is uniquely adapted to interpretation of calculated currents in orbital terms. Figure 4 shows the  $\pi/\pi^*$  energy level diagrams for benzene- and COT-superphanes. In each case, the monocycle levels, which can be classified by orbital angular momentum,  $\Lambda$ , about the principal axis, spread into “bands” containing bonding and antibonding components of opposite  $g/u$  parity. In the benzene system, interaction of two closed shells leads to a closed shell in the superphane/dimer with levels up to and including  $\Lambda = 1$  filled, as in the monocycle. In the COT-based system, interactions of open shells in  $D_{8h}$  symmetry leads to a closed-shell superphane/dimer, with occupation of all orbitals with  $\Lambda \leq 1$  and of the bonding half of the orbitals with  $\Lambda = 2$ . This partial occupation of a  $\Lambda$  shell is analogous to the Jahn–Teller split configuration of planar COT (constrained to the plane, COT adopts bond-alternated

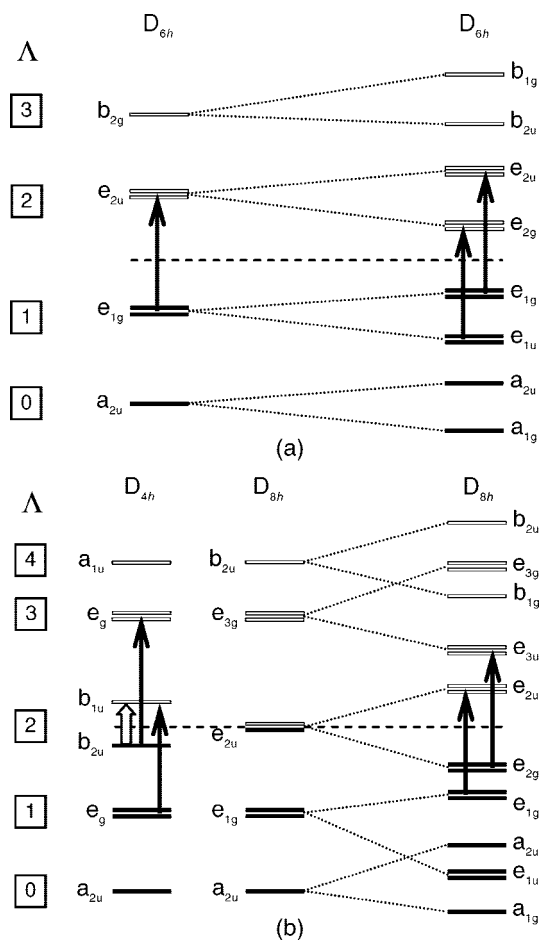


**Figure 4.** Energy level correlation diagram for (a)  $[1_6](1,2,3,4,5,6)$ cyclophane and  $D_{6h}$  benzene and (b) for  $[1_8](1,2,3,4,5,6,7,8)$ cyclophane,  $D_{8h}$  and  $D_{4h}$  planar COT. Solid black arrows show the translationally allowed transitions, and unfilled arrows show the sole rotationally allowed transition. Occupied levels are indicated by solid lines and unoccupied levels by empty boxes.

$D_{4h}$  symmetry with a small splitting between  $\Lambda = 2$  components<sup>8</sup>).

However, monomer and dimer configurations have profoundly different implications for ring current and aromaticity. In a delocalized system with high-order rotational symmetry, two selection rules are obeyed by occupied orbital contributions within the ipsocentric approach. A virtual excitation contributes a diatropic (paratropic) current if the product of symmetries of the initial and target orbitals contains the symmetry of a translation perpendicular to the principal axis (a rotation about that axis). Excitations may be allowed under both, either or neither rules, and intensity of the current will be greater for smaller differences in orbital energies. For monocycles, these rules reduce to an angular momentum criterion: diatropic currents arise from excitations with  $\Delta\Lambda = +1$ , paratropic currents from excitations with  $\Delta\Lambda = 0$ . In  $(4n + 2)$  cycles the sole active excitation is the translationally allowed HOMO–LUMO excitation. In  $4n$  cycles the dominant excitation is the rotationally allowed

HOMO–LUMO excitation over the Jahn–Teller splitting; this masks additional translationally allowed excitation from HOMO and HOMO-1<sup>8</sup> (see Figure 4(b)).

In the dimeric stacks of  $D_{6h}/D_{8h}$  symmetry, parity under inversion gives an additional restriction. By the geometry of the through-space interaction, bonding and antibonding contributions correlating with a given monocycle orbital have parities opposite and equal to that of the parent orbital. Rotational transitions between filled bonding and empty antibonding components with equal  $\Lambda$ , are now forbidden, leaving only the underlying diatropic excitations that were overwhelmed in the monocycle by intense paratropic current. This extra selection rule explains the absence of paratropic current density in  $[1_8](1,2,3,4,5,6,7,8)$ cyclophane, and hence the quenching of  $4n\pi$  antiaromaticity. The consequences for translational transition are less dramatic. Excitations between bands of levels that differ by one unit in  $\Lambda$  are still allowed, but between orbitals of opposite parity, i.e., bonding to bonding and antibonding to antibonding components, ruling out half of the band-to-band excitations predicted by direct analogy with the monocycle.

Application of these symmetry rules to the frontier orbitals of the superphanes gives the transitions illustrated in Figure 4. In each molecule, two magnetically active  $\pi$  orbital pairs, each with a translationally allowed excitation to a unique target pair, account exactly for the earlier observations on the computations of current density, and in particular rationalize the magnetic aromaticity arising from face-to-face through-space interaction of two  $4n\pi$  COT rings.

This rationalization in terms of band-to-band excitations can be continued to taller stacks of rings. For a model stack of  $N$   $(4n + 2)\pi$  rings,  $N$  degenerate pairs of orbitals, descended from the HOMO pairs of the isolated rings, contribute a cylindrical stack of diatropic ring currents above, between and below the rings. (For the benzene trimer, see Figure S5, Supporting Information).

For a model stack of  $N$   $(4n)\pi$  rings, the analysis for even  $N$  is similar to that for the COT dimer, although some band overlap occurs. Two degenerate pairs of orbitals, descended from the nonbonding orbitals of  $D_{8h}$  COT, give rise to a cylindrical diatropic current, with significant current flowing in the space between rings, attenuating as  $N$  increases (see Figure S6, Supporting Information, for  $N = 4$ ,  $n = 2$  case). For odd  $N$ , Jahn–Teller distortion opens up narrow HOMO–LUMO gaps spanned by rotational excitations, leading to paratropic ring currents as in  $D_{4h}$  constrained COT.

**Acknowledgment.** D.E.B. thanks EPSRC for financial support, and P.W.F. thanks the Royal Society/Wolfson scheme for a Research Merit Award. Prof. C. A. Hunter FRS (Sheffield) is thanked for a helpful discussion.

**Supporting Information Available:** Figures S1–S6, geometries and energies of the constrained dimers. This material is available free of charge via the Internet at <http://pubs.acs.org>.

OL802417N